Lattice Boltzmann Analysis of Fluid-Structure Interaction with Moving Boundaries

Alessandro De Rosis[1,*], Giacomo Falcucci[2], Stefano Ubertini[3], Francesco Ubertini[1] and Sauro Succi[4]

[1] *Department of Civil, Environmental and Materials Engineering, University of Bologna, Bologna 40136, Italy.*
[2] *Department of Technologies, University of Naples "Parthenope", Naples, Italy.*
[3] *DEIM - Industrial Engineering School, University of Tuscia, Largo dell'Università s.n.c., 01100, Viterbo, Italy.*
[4] *Istituto per le Applicazioni del Calcolo - CNR, Via dei Taurini, 00100 Roma, Italy.*

Abstract. This work is concerned with the modelling of the interaction of fluid flow with flexibly supported rigid bodies. The fluid flow is modelled by Lattice-Boltzmann Method, coupled to a set of ordinary differential equations describing the dynamics of the solid body in terms its elastic and damping properties. The time discretization of the body dynamics is performed via the Time Discontinuous Galerkin Method. Several numerical examples are presented and highlight the robustness and efficiency of the proposed methodology, by means of comparisons with previously published results. The examples show that the present fluid-structure method is able to capture vortex-induced oscillations of flexibly-supported rigid body.

1 Introduction

The correct prediction of the interaction between a solid structure and a fluid flow is a problem of great interest both from a theoretical and a practical point of view [1,2]. Several industrial, technological, biological and environmental problems are, in fact, associated with Fluid-Structure Interaction (FSI) and the ability of predicting the fluid and solid behavior in such processes is extremely important for these applications. This, together with the increased computer power of the last two decades, is promoting an enormous

---

*Corresponding author. *Email addresses:* `alessandro.derosis@unibo.it` (A. De Rosis), `falcucci@uniroma3.it` (G. Falcucci), `stefano.ubertini@uniparthenope.it` (S. Ubertini), `francesco.ubertini@unibo.it` (F. Ubertini), `succi@iac.cnr.it` (S. Succi)

research effort in this field of computational mechanics. Being this a typical "coupled field" problem, monolithic (i.e. fluid and solid equations solved simultaneously) or partitioned (i.e. each physical field is separately discretized and numerically solved) approaches can be used, being the latter of simpler implementation and presently the only one applicable to practical problems [3–6]. In this paper the fluid flow is modelled by the Lattice-Boltzmann Method (LBM), which is a numerical approach for fluid dynamic investigation based on Boltzmann's Kinetic Equation [7,8]. In recent years, the LBM has been successfully adopted for the simulation of phenomena of technical interest, such as multiphase/reacting flows [9–11], cavitation, spray formation and break-up [12] and others. LBM has also been employed in problems of fluid-structure interaction [13–15] and in the framework of immersed boundary approaches [16–19], for the ease and accuracy with which it enables complicated boundary geometries to be processed. In particular, Zhang and his coworkers [11,12] have proposed an immersed boundary-lattice Boltzmann coupling scheme for deformable and moving boundaries and demonstrated it on blood flows with simplified bi-dimensional geometries. A Lattice-Boltzmann based implicit immersed boundary method has been also developed by Hao and Zhu [20] and tested to simulate a flexible and massless filament in a bi-dimensional viscous flow at low Reynolds numbers.

In LBM, a popular scheme for the fluid-structure interaction is based on the 2nd-order accurate bounce-back rule enforcing the no-slip condition on the solid surface [21, 22]. Such a scheme is suitable for the rigid-solid case where the motion of the solid obstacle is determined only by the external force. However, for the elastic-body case where the solid motion is determined by the local stress state, a very fine mesh might be required for high accuracy [14]. Recently Kollmannsberger et al. [23] have presented very interesting results for bi-dimensional fluid-structure interaction obtained by coupling fixed-grid Lattice-Boltzmann fluid solver with p-refinement finite element solid solver. An interface mesh is used to adapt the two different discretizations and a staggered algorithm with subiteration is chosen for the fluid. Solid time integration is performed by the Newmark method.

The method proposed in this paper can be classified as "non-boundary-fitted", as the solid boundaries do not lie on the fluid nodes, similarly to immersed boundaries [24]. Therefore, the main advantage of the present method is the absence of moving meshes, which usually require high computational times, combined to the simplicity and the computational efficiency of the Lattice Boltzmann method for fluid flows. Using the LBM as the fluid solver, in fact, allows moving the body in a fixed lattice, given proper boundary conditions (i.e. Mei et al. [25]) and a refill procedure for fluid node initialization after solid obstacle motion [15, 26, 27]. The dynamics of the rigid body is modelled through the Time Discontinuous Galerkin Method, because of its good accuracy and dissipative properties [28, 29]. The computational cost is successfully reduced owing to the implementation proposed in [28, 29]. Different types of constraints, including rigid and elastic joints are considered and the dynamic response of the rigid obstacle is calculated as a coupled function of the fluid-dynamic external field.

2 Numerical method

2.1 The Lattice Boltzmann method

Our theoretical/computational analysis is based on the lattice Boltzmann equation (LBE), a minimal form of the Boltzmann kinetic equation, which has proven quite successful for the quantitative description of a broad class of complex flow phenomena [7]. Since the LB has been described at length in the current literature, here we shall only revisit the basic ideas behind its formulation. The LB equation reads as follows,

$$f_i(\boldsymbol{x}+\boldsymbol{c}_i\Delta t, t+\Delta t) - f_i(\boldsymbol{x},t) = -\omega(f_i - f_i^{eq})\Delta t, \tag{2.1}$$

where f_i is the probability (density function) of finding a fluid particle at site $\boldsymbol{x}$ at time t, moving along the $i-th$ lattice direction defined by the discrete speeds $\boldsymbol{c}_i$, with $i=0,\cdots,b$. The left-hand side of Eq. (2.1) stands for molecular free-streaming, whereas the right-hand side represents the collisional relaxation towards local Maxwellian equilibrium, on a time-scale $\tau = 1/\omega$.

The local equilibrium is given by the usual expression, in the form of a second-order expansion in the local mach number, $Ma = u/c_s$, of the local Maxwell distribution:

$$f_i^{eq}(\boldsymbol{x};t) = w_i\rho\left(1 + \frac{\boldsymbol{v}\cdot\boldsymbol{c}_i}{c_s^2} + \frac{(\boldsymbol{v}\cdot\boldsymbol{c}_i)^2}{2c_s^4} - \frac{\boldsymbol{v}\cdot\boldsymbol{v}}{2c_s^2}\right), \tag{2.2}$$

where

$$\rho(\boldsymbol{x};t) = \sum_i f_i(\boldsymbol{x};t) \tag{2.3}$$

is the fluid density, and

$$\boldsymbol{v}(\boldsymbol{x};t) = \frac{\sum_i f_i(\boldsymbol{x};t)\boldsymbol{c}_i}{\rho(\boldsymbol{x};t)} \tag{2.4}$$

is the flow velocity.

In this work we refer to the D2Q9 particles speed model: a standard 9-speed, two-dimensional lattice, with $b=8$ (including a zero-speed particle).

2.2 Time integration scheme for the solid structure

The equation of motion of a deformable solid discretized using, for example, the finite element method reads as follows:

$$\mathbf{M\ddot{u}} + \mathbf{C\dot{u}} + \mathbf{Ku} = \mathbf{F}, \tag{2.5}$$

where $\mathbf{u}$ is a vector of n components describing the displacements of the solid and $\mathbf{M}$, $\mathbf{C}$ and $\mathbf{K}$ are $n\times n$ matrices, representing the mass, damping and stiffness of the structure, respectively. The dot symbol ($\dot{}$) indicates the time derivative.
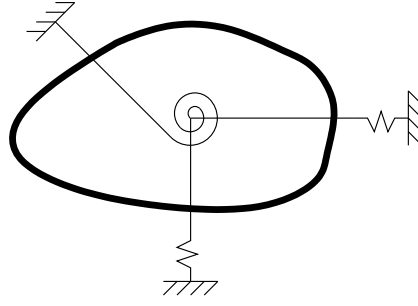
Figure 1: Rigid body.

By restricting to rigid body dynamics (see Fig. 1) the time-dependent loads on the structure are given by

$$\mathbf{R}(t) = \oint_{\partial\Omega} \sigma \mathbf{n} dS, \qquad \mathbf{M}(t) = \oint_{\partial\Omega} \mathbf{r} \times \sigma \mathbf{n} dS, \qquad (2.6)$$

where σ is the fluid stress tensor, acting upon the boundary $\partial\Omega$ of the solid, with outer unit normal $\mathbf{n}$, and $\mathbf{r}$ is the distance from the center of mass.

In two-dimensional conditions, the equation of motion (2.5) reduces to the following three equations

$$m_i \ddot{u}_i + c_i \dot{u}_i + k_i u_i = R_i, \qquad i = x, y, \qquad (2.7a)$$

$$I_\theta \ddot{\theta} + c_\theta \dot{\theta} + k_\theta \theta = M, \qquad (2.7b)$$

where x and y are the in-plane directions, the displacements u_i are the rigid translations and θ represents the rigid rotation. The scalar quantities m_i, c_i, k_i, I_θ, c_θ, k_θ denote mass, damping and stiffness moduli for the translational and rotational degrees of freedom; R_i are the in-plane components of the resultant force vector $\mathbf{R}$ and M is the in-plane component of the resultant moment $\mathbf{M}$.

The above equations are integrated in time using the Time Discontinuous Galerkin Method (TDG) [28, 29]. It is a one-step method that possesses higher order accuracy in the low-frequency modes and effective dissipation in the high-frequency ones. In particular, piecewise linear time interpolants are adopted for both displacements and velocities, assumed as independent variables. The approximations may be discontinuous at time levels t_n, as illustrated schematically in Fig. 2.

Selecting linear test functions $\mathbf{w}_u$ and $\mathbf{w}_v$ the TDG formulation for the typical time interval is given by the following condition that should be satisfied for any test function:

$$\int_{t_n}^{t_{n+1}} \mathbf{w}_v^{\mathrm{T}} (\mathbf{M}\ddot{\mathbf{u}} + \mathbf{C}\dot{\mathbf{u}} + \mathbf{K}\mathbf{u} - \mathbf{F}) dt$$

$$+ \int_{t_n}^{t_{n+1}} \mathbf{w}_u^{\mathrm{T}} \mathbf{K}(\dot{\mathbf{u}} - \mathbf{v}) + \mathbf{w}_u^{\mathrm{T}}(t_n) \mathbf{K}[\![\mathbf{u}(t_n)]\!] + \mathbf{w}_v^{\mathrm{T}}(t_n) \mathbf{M}[\![\mathbf{v}(t_n)]\!] = 0, \qquad (2.8)$$
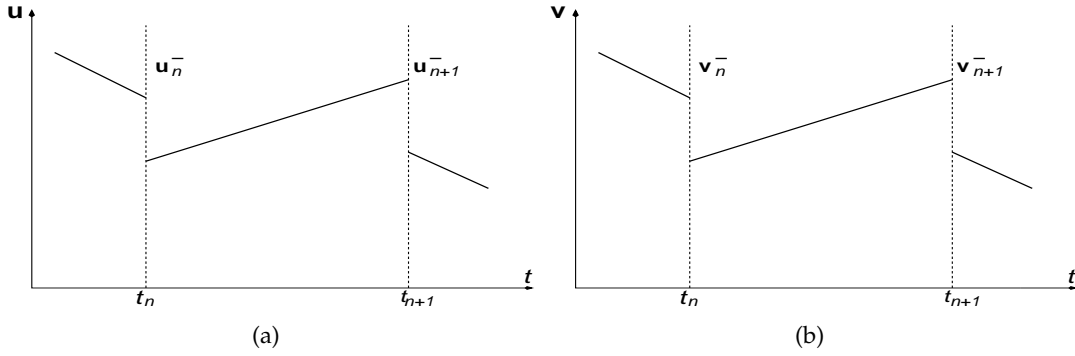
Figure 2: Time approximation for solid displacements and velocities.

where $[\![\mathbf{u}(t_n)]\!]$ and $[\![\mathbf{v}(t_n)]\!]$ are the jumps of the approximate solution for displacements and velocities at $t = t_n$. The above condition enforces, in a weak sense, the equation of motion, the relation between displacement and velocity and the initial conditions for the typical time interval.

It can be proved that in linear regime the resultant TDG algorithm is third-order accurate, unconditionally stable and asymptotically annihilating in the high-frequency range (*L*-stable). Indeed, a recent work presents an improved TDG version that retains these properties for non-linear dynamics as well [29]. Despite these good properties, the major drawback is the computational cost, which is here successfully reduced through the implementation proposed in [28]. This approach is based on the following iterative scheme:

$$\begin{cases} \mathbf{M}^*\bar{\mathbf{v}}_k^{(l+1)} = \mathbf{F}_k^* - \mathbf{C}\tilde{\mathbf{v}}_k^{(l+1)} - \mathbf{K}\tilde{\mathbf{u}}_k^{(l+1)}, \\ \bar{\mathbf{u}}_k^{(l+1)} = \tilde{\mathbf{v}}_k^{(l+1)} + \nu\Delta t\bar{\mathbf{v}}_k^{(l+1)}, \end{cases} \qquad k = 0,1. \tag{2.9}$$

In the above equation, predictor displacements $\tilde{\mathbf{u}}_k$ and velocities $\tilde{\mathbf{v}}_k$ are defined as

$$\tilde{\mathbf{v}}_0^{(l+1)} = \bar{\mathbf{v}}_n + \beta\Delta t(\bar{\mathbf{v}}_0^{(l)} - \bar{\mathbf{v}}_1^{(l)}), \tag{2.10a}$$

$$\tilde{\mathbf{u}}_0^{(l+1)} = \bar{\mathbf{u}}_n + \beta\Delta t(\bar{\mathbf{u}}_0^{(l)} - \bar{\mathbf{u}}_1^{(l)}) + \nu\Delta t\tilde{\mathbf{v}}_0^{(l+1)}, \tag{2.10b}$$

$$\tilde{\mathbf{v}}_1^{(l+1)} = \bar{\mathbf{v}}_n + (1-\nu)\Delta t\bar{\mathbf{v}}_0^{(l+1)}, \tag{2.10c}$$

$$\tilde{\mathbf{u}}_1^{(l+1)} = \bar{\mathbf{u}}_n + (1-\nu)\Delta t\bar{\mathbf{u}}_0^{(l+1)} + \nu\Delta t\tilde{\mathbf{v}}_1^{(l+1)}, \tag{2.10d}$$

where the effective mass matrix $\mathbf{M}^*$ and load vectors $\mathbf{F}_k^*$ are given by

$$\mathbf{M}^* = \mathbf{M} + \nu\Delta t\mathbf{C} + \nu^2\Delta t^2\mathbf{K}, \tag{2.11a}$$

$$\mathbf{F}_0^* = \frac{1}{4}\left[(3\sqrt{2}-2)\mathbf{F}_0 + 3(2-\sqrt{2})\mathbf{F}_{2/3}\right], \tag{2.11b}$$

$$\mathbf{F}_1^* = \frac{1}{2}(3\mathbf{F}_{2/3} - \mathbf{F}_0). \tag{2.11c}$$

$\mathbf{F}_0$ and $\mathbf{F}_{2/3}$ are the values of the load vector $\mathbf{F}$ at $t=t_n$ and $t=t_n+2/3\Delta t$, respectively, and the coefficients ν and β are fixed to [28]:

$$\nu=1-\frac{\sqrt{2}}{2}, \qquad \beta=\sqrt{2}-\frac{4}{3}. \tag{2.12}$$

Displacements and velocities at the end of the current time step are given by

$$\mathbf{v}_{n+1}=\bar{\mathbf{u}}_1^{(l)}, \qquad \mathbf{u}_{n+1}=\bar{\mathbf{u}}_n+\Delta t\left[(1-\nu)\bar{\mathbf{u}}_0^{(l)}+\nu\bar{\mathbf{u}}_1^{(l)}\right]. \tag{2.13}$$

Notice that vectors $\bar{\mathbf{v}}_k$ are computed using the same matrix $\mathbf{M}^*$, that can be factorized only once.

It can be proved that the iterative scheme converges and, in particular, two iterations ($l=2$) are sufficient to get third-order accuracy and L-stability. Indeed, the first iteration ($l=1$) reduces to the Nørset algorithm [30], that is second-order accurate and L-stable.

The present approach offers also the advantage of two embedded error estimates. The first is obtained by comparing the second-order accurate solution of the first iteration with the third-order accurate solution of the second one. The second error estimate is the jump of the approximate solution at the beginning of the current time step, which gives a valuable information about the amount of numerical dissipation [31].

2.3 Fluid-solid coupling scheme

The LB fluid and TDG solid solvers are coupled through a staggered-explicit coupling strategy, adopting the same time sequence for both solvers.

As a result, at each LB step, the LB solver provides the hydrodynamic load, $\mathbf{F}(t)$, to the structure, while the solid solver restitutes the array of displacements $\mathbf{u}$, which is then used in the formulation of the LB boundary conditions. More precisely, the updated set of displacements is used to compute the new position of the solid boundary, according to the interpolation scheme described in [32].

A sketch of the fluid-solid coupling procedure is provided in Fig. 3.

As to the initialization of fluid nodes uncovered by the solid motion, we employ the refill procedure described in [15].
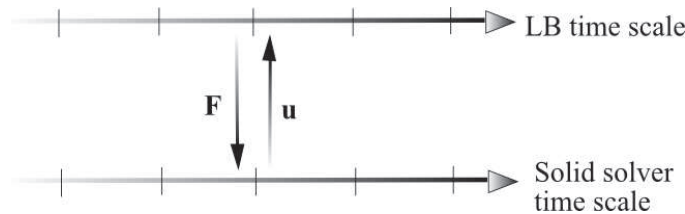

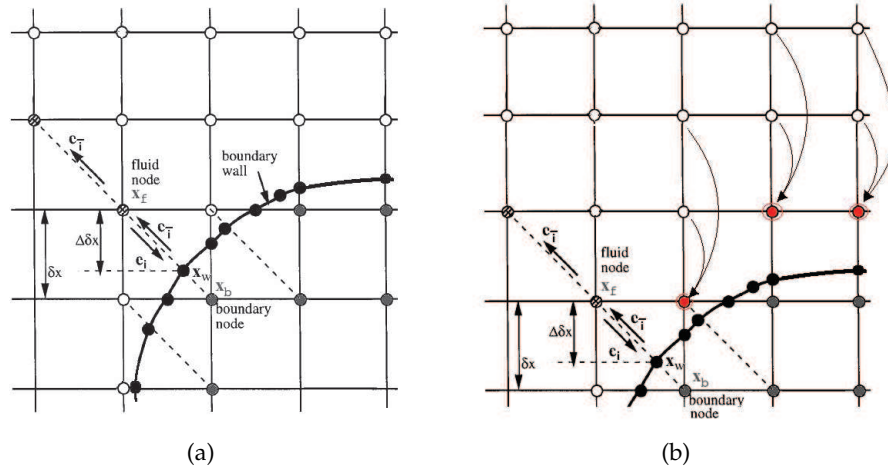Figure 3: Schematic representation of the coupling between the LB fluid solver and the TDG solid solver.

Figure 4: Sketch of the boundary condition scheme for the moving solid object; (b) sketch of the refill procedure.

Lattice nodes immediately close to the obstacle do not participate to the standard LB streaming process as the immersed object acts as a wall for the particles' motion. The motion of the solid obstacle within the background lattice is reconstructed by means of Filippova and Hänel enhanced procedure [25, 32]. We consider the nodes x_f and x_b located immediately *outside* and *inside* the solid object, respectively, see Fig. 4(b). The location x_w on the boundary denotes the intersections of the object boundary with the lattice link between x_f and x_b. The length fraction of the intersected link between x_f and x_w is $\Delta = \|x_f - x_w\| / \|x_f - x_b\|$. The probability density functions of the nodes surrounding the cylinder are recovered by using the linear interpolation proposed in [32], that is,

$$\tilde{f}_{\bar{i}}(x_b,t) = (1-\chi)\tilde{f}_i(x_f,t) + \chi f_i^*(x_b,t) + 2w_i\rho(x_b,t)[c_{\bar{i}} \cdot v(x_w,t)]/c_s^2, \qquad (2.14)$$

where $\tilde{f}$ is the post-collision population, subscript $\bar{i}$ denotes the direction from a wall node x_w to a fluid node x_f, and subscripts i and $\bar{i}$ identify opposite directions. Once the populations are computed according to Eq. (2.14), the standard collision process takes place for all the lattice sites in the computational domain. In Eq. (2.14), $f_i^*(x_b,t)$ is a fictitious equilibrium density function given by

$$f_i^*(x_b,t) = w_i\rho(x_f,t) \left[1 + \frac{c_i \cdot v_*}{c_s^2} + \frac{[c_i \cdot v(x_f,t)]^2}{2c_s^4} - \frac{\|v(x_f,t)\|^2}{2c_s^2}\right]. \qquad (2.15)$$

In Eqs. (2.14) and (2.15), the quantities χ and u_* are determined as follows:

$$\begin{cases} v_* = [(\Delta-1)v(x_f,t)+v(x_w,t)]/\Delta, \quad \chi=[2\Delta-1]/\tau, & \text{if} \quad \Delta \geq 1/2, \\ v_* = v(x_f,t), \quad \chi=[2\Delta-1]/[\tau-1], & \text{if} \quad \Delta < 1/2. \end{cases} \qquad (2.16)$$

An ad-hoc *refill* procedure is adopted for the hydrodynamic quantities of nodes *uncovered* by cylinder motion [15].

According to Fig. 4(b), we initialize the nodes uncovered by the moving obstacle by fixing their populations to the equilibrium ones; to this purpose we need macroscopic density and velocity for these nodes. To compute density and velocity, we *extrapolate* the populations in the uncovered nodes according to the first two fluid neighbours along the object motion direction. Once the populations are fixed, we compute density and velocity according to Eqs. (2.3) and (2.4).

3   Results and discussion

The simulated test case is a uniform flow over an oscillating cylinder that can move only in the direction normal to the inlet velocity. The geometry of the problem and the boundary conditions employed in the simulation are displayed in Fig. 5. The spring is linear, with stiffness $k = 5.79$ N/m and damping factor $c = 0.325$ g/s. The mass and the diameter of the cylinder are $m = 2.979$ g and $D = 0.16$ cm. The fluid is water with viscosity $\mu = 0.01$ g/(cm s) and density $\rho = 1$ g/cm^3.
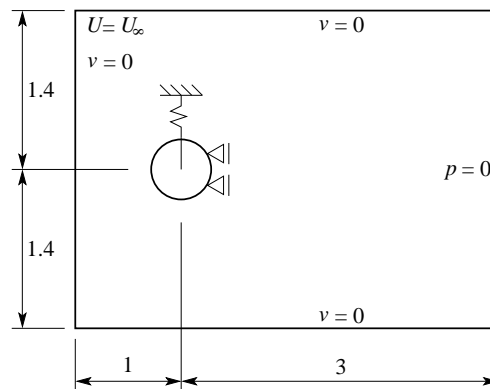

Figure 5: Oscillating cylinder: definition of the problem and associated internal and external boundary conditions. At the inlet, a given mainstream speed U_∞ is prescribed, while at the outlet, zero pressure boundary conditions are imposed. At the upper and lower boundaries, zero-velocity conditions are applied. Zero-velocity conditions are also applied at the moving surface of the cylinder.

Different far-field fluid velocities are considered, such that the Reynolds number, given by $\mathcal{R}e = \rho U_\infty D / \mu$, varies between 90 and 130. In all numerical experiments, the fluid is started from rest conditions $U = 0$. As usual the mainstream speed is denoted by U_∞.

Fig. 6 shows the vortex shedding frequency f_V as a function of the Reynolds, $\mathcal{R}e$, number. The frequency f_V is evaluated from the evolution of the lift coefficient. We indicate with f_N the natural frequency of the rigid body as a mass-spring system ($f_N = \sqrt{k/m}$). Benchmark values are taken from the vortex shedding frequencies associated with the stationary cylinder, as suggested in [33, 34].

Fig. 7 shows the relative amplitude Y/D as a function of the Reynolds number, where Y is the displacement along vertical direction induced by the lift force. The figure clearly
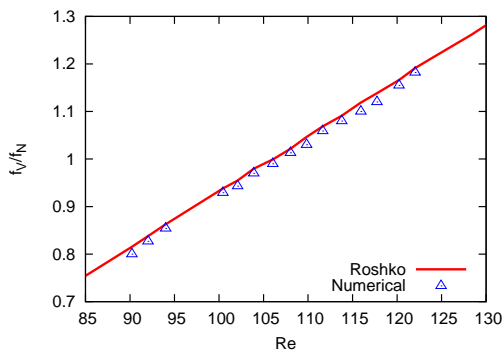
Figure 6: Oscillating cylinder: frequencies vs Reynolds number. The solid line denotes the vortex shedding frequency associated with a stationary cylinder [33, 34].
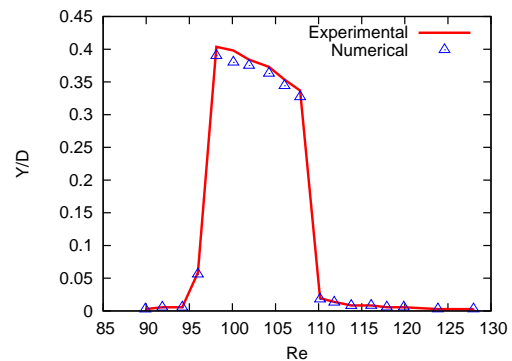
Figure 7: Oscillating cylinder: amplitudes of the vertical motion vs the Reynolds number. The figure clearly displays the onset of a symmetry-breaking instability in the range $95 < \mathcal{R}e < 110$, in close agreement with experimental results (solid line) [35].

shows the onset of a symmetry-breaking instability in the range $95 < \mathcal{R}e < 110$, in close agreement with the experimental data obtained in [35].

At the low Reynolds number end of the lock-in region, the oscillations start with a sudden jump-up. As the Reynolds number increases, the amplitude of the oscillations smoothly decreases so that the jump-down at the upper end of the lock-in region is less significant. Figs. 6 and 7 show a good agreement between our results and literature data, thereby lending credit to both numerical model and the coupling algorithm present in this work [33–35].

In Figs. 8(b) and 9(b), we report the behaviour of the oscillating cylinder in the frequency domain, as obtained by Fourier transforming the time sequence of the center-mass displacement. The graphs show the amplitude spectrum of Y/D, as obtained by a Fast Fourier Transform of the data represented in Figs. 8(a) and 9(a) vs frequency. It should be remarked that for the latter figure, the Fourier transform is taken after the transient is exhausted ($t > 100$ s). From these figures, it is apparent that up to $\mathcal{R}e = 120$, the spectrum gives no sign of multi-mode locking, i.e. the frequency spectrum remains highly peaked around a single frequency.

On a standard PC (Intel I7-920, frequency clock 2.6GHz, 8 cores, 8 MB cache L3, 8 GB RAM), the method takes about 0.05 CPU seconds per time step, for a LB grid of 350×220 lattice sites, slightly higher (about 10%) than the computational time needed for the flow over a fixed cylinder. The computational cost is mainly due the fluid-solid boundary condition.

The computational cost due to the fluid solver is negligible, due to the fact that the rigid body motion is described by a single degree of freedom. The procedure described in this paper is suited to handle a generic class of constraints and any number of solid degrees of freedom. In particular, fluid interaction with multi-bodies or elastic structures discretized by the finite element method could be investigated using the present frame-
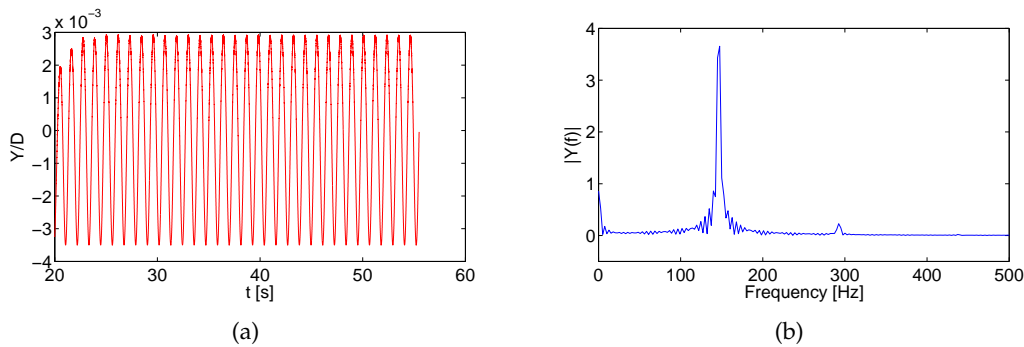
Figure 8: Oscillating cylinder at $\mathcal{R}e = 90$: (a) amplitudes, (b) FFT of amplitude signal in frequency domain.
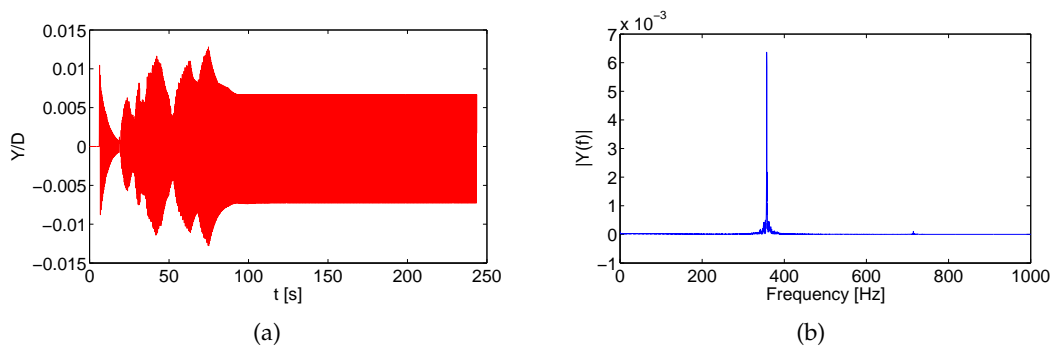

Figure 9: Oscillating cylinder at $\mathcal{R}e = 120$: (a) amplitudes, (b) FFT of amplitude signal in frequency domain.

work. As regards the computational cost, when the number of solid degrees of freedom increases the solid solver could contribute significantly to the overall cost. The study of more complex fluid-structure problems is currently under investigation.

4   Conclusions

Summarizing, in this work we have presented an adapting LB for an established FSI coupling scheme employing TDG, based on the combination of the Lattice Boltzmann (LB) method for the fluid and the Time Discontinuous Galerkin (TDG) method time-marching scheme for the solid degrees of freedom. The LB-TDG scheme is demonstrated for the case of an oscillating cylinder, and shows to provide satisfactory agreement with existing literature data, both numerical and experimental. The methodology presented here is fairly general and can describe a broad class of two-dimensional fluid-solid problems, including deformable bodies, without the need of moving meshes. This makes the computational time comparable to that needed for modelling the flow over a fixed cylinder. It is important to note that the proposed method (i.e. curved boundaries combined to a proper refill procedure) is independent from the geometry of the boundaries (i.e. the

body is somehow "immersed" in the lattice). Therefore, the gain with respect to traditional FSI is expected to grow with growing body shape complexity (i.e. typical engineering problems). The extension of the present coupling scheme to three-dimensional problems, although computationally intensive, does not appear to pose any conceptual problem, and will be explored in the future.

Acknowledgments

References

[1] E. Naudascher Rockwell. Practical Experiences with Flow-Induced Vibrations. Springer, 1980.
[2] H. Morand and R. Ohayon. Fluid Structure Interaction. John Wiley and Sons, New York, 1995.
[3] F.J. Blom. A monolothical fluid-structure interaction algorithm applied to the piston problem. Comp. Meth. Appl. Mech. Engr., 167:369–391, 1998.
[4] B. Hübne, E. Walhorn, and Dinkler D. A monolithic approach to fluid-structure interaction using space-time finite elements. Comp. Meth. Appl. Mech. Engr., 193:2087-2104, 2004.
[5] G.P. Guruswamy. A review of numerical fluids/structures interface methods for computations using high-fidelity equations. Comp. Struct., 80(1):31–41, 2002.
[6] C. Wood, A.J. Gil, O. Hassan, and J. Bonet. Partitioned block-Gauss-Seidel coupling for dynamic fluid-structure interaction. Comp. Struct., 88(23-24):1367–1382, 2010. Special Issue: Association of Computational Mechanics, United Kingdom.
[7] R. Benzi, Succi S., and M. Vergassola. The lattice Boltzmann equation: Theory and applications. Phys. Rep., 222:145–197, 1992.
[8] S. Succi. The Lattice Boltzmann Equation for Fluid Dynamics and Beyond. Clarendon, Oxford, 2001.
[9] S. Chibbaro, G. Falcucci, G. Chiatti, H. Chen, X. Shan, and S. Succi. Lattice Boltzmann models for nonideal fluids with arrested phase-separation. Phys. Rev. E, 77, 036705, 2008.
[10] G. Falcucci, S. Ubertini, and S. Succi. Lattice Boltzmann simulations of phase-separating flows at large density ratios: the case of doubly-attractive pseudo-potentials. Soft Matter, 6:4357–4365, 2010.
[11] G Falcucci, S. Ubertini, C. Biscarini, S. Di Francesco, D. Chiappini, S. Palpacelli, A. De Maio, and S. Succi. Lattice Boltzmann methods for multiphase flow simulations across scales. Comm. Comput. Phys., 9:269–296, 2011.
[12] G. Falcucci, G. Bella, S. Ubertini, S. Palpacelli, and A. De Maio. Lattice Boltzmann modeling of Diesel spray formation and break-up. SAE Int. J. Fuels Lubr., 3:582–593, 2010.
[13] D. Qi and C.K. Aidun. A new method for analysis of the fluid interaction with a deformable membrane. J. Stat. Phys., 90:145, 1998.
[14] X. Shi and N. Phan-Thien. Distributed lagrange multiplier/fictitious domain method in the framework of lattice Boltzmann method for fluid-structure interactions. J. Comp. Phys., 206:81–94, 2005.

[15] G. Falcucci, M. Aureli, S. Ubertini, and M. Porfiri. Transverse harmonic oscillations of laminae in viscous fluids: A lattice Boltzmann study. Phil. Trans. Royal Soc. A, 369(1945):2456–2466, 2011.

[16] Z.G. Feng and E.E. Michaelides. The immersed boundary-lattice Boltzmann method for solving fluid-particles interaction problems. J. Comp. Phys., 195:602–628, 2004.

[17] Y. Cheng and H. Zhang. Immersed boundary method and lattice Boltzmann method coupled FSI simulation of mitral leaflet flow. Computers & Fluids, 39:871–881, 2010.

[18] J. Hao and L. Zhu. A lattice Boltzmann based implicit immersed boundary method for fluid-structure interaction. Comp. Math. App., 59:185–193, 2010.

[19] K. Suzuki and T. Inamuro. Effect of internal mass in the simulation of a moving body by the immersed boundary method. Computers & Fluids, 49:173–187, 2011.

[20] J. Hao and L. Zhu. A lattice boltzmann based implicit immersed boundary method for fluid-structure interaction. Comp. Math. Appl., 59(1):185–193, 2010.

[21] A.J.C. Ladd. Numerical simulation of particulate suspensions via a discretized Boltzmann equation, part 1. Theoretical foundation. J. Fluid Mech., 271:285, 1994.

[22] A.J.C. Ladd. Numerical simulation of particular suspensions via discretized Boltzmann equation, part 2. Numerical results. J. Fluid Mech., 271:311–339, 1994.

[23] S. Kollmannsberger, S. Geller, A. Düster, J. Tölke, C. Sorger, M. Krafczyk, and E. Rank. Fixed-grid fluid-structure interaction in two dimensions based on a partitioned Lattice Boltzmann and *p*-fem approach. Int. J. Numer. Meth. Engr., 79(7):817–845, 2009.

[24] C. S. Peskin. Flow patterns around heart valves: A numerical method. J. Comp. Phys., 10(2):252–271, 1972.

[25] R. Mei, L.-S. Luo, and W. Shyy. An accurate curved boundary treatment in the lattice Boltzmann method. J. Comp. Phys., 155:307–330, 1999.

[26] P. Lallemand and L.-S. Luo. Lattice Boltzmann method for moving boundaries. J. Comp. Phys., 184:406–421, 2003.

[27] A. Caiazzo. Analysis of lattice Boltzmann nodes initialisation in moving boundary problems. Progress Comp. Fluid Dyn., 8:3–10, 2008.

[28] M. Mancuso and F. Ubertini. An efficient integration procedure for linear dynamics based on a time discontinuous Galerkin formulation. Comp. Mech., 32:154–168, 2003.

[29] M. Mancuso and F. Ubertini. An efficient time discontinuous Galerkin procedure for nonlinear structural dynamics. Comp. Meth. Appl. Mech. Engr., 195(44-47):6391–6406, 2006.

[30] M. Mancuso and F. Ubertini. The Nørsett time integration methodology for finite element transient analysis. Comp. Meth. Appl. Mech. Engr., 191:3297–3327, 2002.

[31] L. Govoni, M. Mancuso, and F. Ubertini. Hierarchical higher-order dissipative methods for transient analysis. Int. J. Numer. Meth. Engr., 67:1730–1767, 2006.

[32] O. Filippova and D. Hänel. Lattice Boltzmann simulation of gas-particle flow in filters. Computers & Fluids, 26:697–712, 1997.

[33] A. Roshko. On the development of turbulent wakes from vortex streets. National Advisory Committee for Aeronautics, NACA, page 2913, 1953.

[34] W. Dettmer and D. Peric. A computational framework for fluid-rigid body interaction: Finite element formulation and applications. Comp. Meth. Appl. Mech. Engr., 195(13-16):1633–1666, 2006.

[35] P. Anagnostopoulos and P. W. Bearman. Response characteristics of a vortex excited cylinder at low Reynolds numbers. J. Fluids Struct., 6:39–50, 1992.